INTERPRETATION OF GAMMA-RAY LOGS OF THE STRATIFIED OIL SHALE SEAM IN THE ATTARAT UM GHUDRAN DEPOSIT, CENTRAL JORDAN

JÜRI PLADO[(a)*], STELLA OTS[(a)], VÄINO PUURA[(a)], HARDI AOSAAR[(b)]

[(a)] Institute of Ecology and Earth Sciences, University of Tartu, Ravila 14A, 50411 Tartu, Estonia
[(b)] Eesti Energia AS, Lelle 22, 11318 Tallinn, Estonia

Abstract. *The study analyses gamma-ray logging data (NGAM) collected by the Attarat Power Company (APCO; a subsidiary of Enefit) about 16 coring boreholes drilled in its exploration area in the Attarat Um Ghudran oil shale (OS) deposit, central Jordan during 2008–2013. Data are compared with lithostratigraphic information that is based on the visual and chemical description of cores. The original natural gamma radiation data were not corrected for the (unspecified) drill hole diameter or casing, thus, the amplitudes of signals were incomparable. The study analyses the raw data in order to produce a master log that could be used for stratigraphic purposes within the Attarat Um Ghudran and, possibly, the neighbouring deposits in future. The creation of a master log is based on the data about 16 individual logs and stratigraphic descriptions. It was possible as the deposit is monoclinally layered, and there exist radiogenic anomalies of primary sedimentation origin. A master log was produced by comparing the averaged signals (with radiuses of 1 and 2.5 m) with each other and producing a binary (bar code-like) log based on their relationship. Such a method describes wavelengths of natural gamma radiation intensity for preference, without considering its absolute values. Interpretation was tested comparing gamma-ray logs and stratigraphic data about three drill holes. The results confirmed geologically determined stratigraphic boundaries of layers with reasonable accuracy (the standard error of predicted depths ≤ 0.76 m). The method enables one to partly replace the coring-sampling-laboratory testing complex with a more cost-effective percussion drilling followed by gamma-ray logging.*

Keywords: *Attarat Um Ghudran, Jordan oil shale, gamma-ray logging, stratigraphy.*

---

* Corresponding author: e-mail *juri.plado@ut.ee*

1. Introduction

Characteristic energy sources in Jordan are renewable energy and oil shale (OS). Natural gas potential has been found in some areas, but over 90 % of the country's energy is imported [1]. Oil shale is the only local energy resource which is able to reduce Jordan's dependence on imported crude oil and natural gas [2]. With over 34 billion barrels of OS resources accumulated in 23 known surface and near-surface deposits (Fig. 1), Jordan ranks 7th in the world for the geological resources of this rock [3]. Eight of these deposits, i.e. Jurf ed Darawish, Sultani, Wadi Maghar, El Lajjun, Attarat Um Ghudran, Khan el Zabib, Siwaga and Wadi Thamad, are located in west-central Jordan and have been investigated to different degrees. El Lajjun, Sultani, Attarat Um Ghudran and Wadi Maghar are the major deposits of commercial interest. This work focuses on the Attarat Um Ghudran deposit that is located 34 km east of the village of Al Qatrana in the Central Jordanian Limestone Physiographic Province [4].

Oil shale is defined as a sedimentary rock whose solid immature organic matter (OM) is insoluble in organic solvents, but forms liquid oil-like hydro-carbons when subjected to distillation at temperatures up to 500–600 °C. Jordanian OS is described as a kerogen-rich sedimentary rock (mostly carbonates, chalk, marl and shale) that was formed in a shallow marine shelf during the Maastrichtian, Paleocene and early Eocene [5]. The source of kerogen is marine algae. Burial conditions, heat and pressure caused the OM to change to kerogen. The high levels of kerogen content, location of
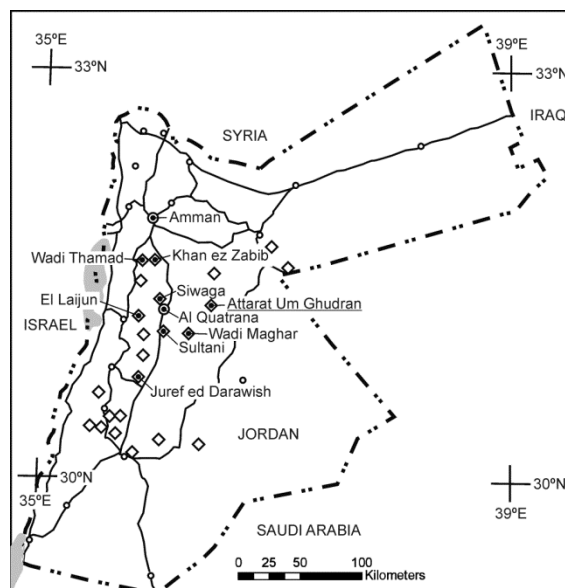

Fig. 1. Oil shale occurrence in Jordan (after [3]). Deposits and settlements are indicated by diamonds and circles, respectively.

deposits near potential consumers and applicability of surface mining technique promotes utilization of Jordanian OS [6].

The Attarat Um Ghudran deposit was first reported by Sunna in 1984 [7]. The discovery took place during the exploration activities within the framework of the geological mapping project carried out by the Natural Resources Authority, The Hashemite Kingdom of Jordan. It was found that the deposit was situated within the Upper Cretaceous chalk marl belt (Muwaqqar Chalk and Marl Formation (MCM)). The rocks forming the deposit and the overburden (OB) of variable thickness were found to be composed of marl, chalk, limestone and chert. Based on 85 to 145 m long drill holes spaced from 4 to 6 km apart, the thicknesses of OS and OB were discovered to vary from 10 to 90+ m and from 45 to 62+ m, respectively [6, 8]. At that time, 1984, the OS bodies were found to form big elongated lenses.

Using a variety of field and laboratory techniques [9], an updated Attarat Um Ghudran OS seam classification (Table 1) was given recently by Puura et al. [10]. It is based on the classification [11] that considered Syrian and Jordanian oil shales as marine mudstones. The total succession of the OS unit, rarely up to 112 m thick, is divided into eight OS layers (from bottom to top, indexed as A, B1, B2, C, D, E1, E2, E3), including three diagenetic dolomitic limestone interlayers in between (A/B, B/C and D/E). Structurally, two main types of OS dominate: (i) thinly bedded (laminated) to almost massive mudstone composed of variably calcareous to siliceous very fine-grained shale and (ii) more-or-less dense alternation of thin beds of mudstone and < 2 mm thick microbeds, lenses or laminae of dominantly carbonate grain-bearing wackestone or seldom packstone (visually up to 70%) [10]. The deposit is covered by the calcareous Eocene Um Rijam Chert (URC) Limestone Formation. Below URC, OS is weathered with variable thickness. The weathered oil shale (WOS) is composed of the mineral residue left over after the oxidation of OM and sulphide minerals [10], and, together with URC, forms OB for the fresh (unweathered) oil shale (FOS). Lithologically, WOS consists of chalk rock with minor chalky limestone and clayey silt or clay interbeds.

The main objective of the present study was to check whether the gamma intensity of the OS seam has common features in vertical direction in different parts of the APCO's exploration area. A further task was to produce a scheme that could be applied for stratigraphic purposes by using gamma-ray data alone, and check its accuracy. Such a scheme would allow employing a cost-effective combination of percussion drilling and gamma-ray logging in appropriate cases. The present study was based on lithostratigraphic and gamma logging data (NGAM) collected by APCO about 16 boreholes. The boreholes for analyses were chosen by the company and their names are encoded.

Table 1. Lithostratigraphic and bar log division of the oil shale seam, APCO exploration area, Attarat Um Ghudran Deposit

Layer	Thickness, m	Bar code	Thickness, m	Bar code	Thickness, m
E3	44.38	E11	2.75		
		E10	0.89	e10	2.68
		E9	2.44	e9	2.92
		E8	2.00	e8	1.92
		E7	1.03	e7	1.75
		E6	2.53	e6	2.00
		E5	1.55	e5	2.93
		E4	1.82	e4	2.13
		E3	1.58	e3	2.07
				e2	4.42
E2	2.90	E2	2.38		
E1	7.27	E1	3.12	e1	2.59
D/E	1.40			d2	2.09
D	5.23	D2	1.97		
		D1	0.92	d1	1.11
				c2	2.12
C	9.10	C2	2.18		
		C1	1.83	c1	2.94
B/C	0.61			b6	1.76
B2	15.54	B6	2.49		
		B5	1.07	b5	2.03
		B4	4.13	b4	1.71
				b3	4.20
B1	7.37	B3	2.01		
		B2	1.14	b2	1.14
		B1	1.17	b1	1.61
A/B	0.71			a3	2.36
A	10.24	A3	2.09		
		A2	1.91	a2	1.31
		A1	2.26	a1	2.14

2. Gamma-ray logging

Well logging is a geophysical prospecting technique which measures the physical properties of rocks with a sensor positioned in a borehole. It is an alternate to the analysis of cores, side-wall samples and cuttings. The aim of gamma-ray logging is to measure natural gamma radiation emitted by the radioactive isotopes of uranium (U), thorium (Th) and potassium (K) causing the highest gamma-ray values for shales, including organic rich ones, and volcanic ash. Low values are found in anhydrite, coal, clean sandstones, dolomite, limestone and halite. As Attarat Um Ghudran is an OS deposit, then the natural gamma logging method is suitable to be used for identification of its stratigraphy and lithology.

Gamma-ray logging has some limitations that reduce the accuracy of the obtained data. Interpretation of a log may be influenced by such factors as

borehole geometry, casing material and configuration, and drilling mud density. For instance, the density of the drilling mud can affect the signal. So, the higher the density of the mud, the higher the attenuation of the gamma radiation and the greater the underestimation of gamma counts. This is due to the increased Compton scattering in the drilling mud. Potassium chloride-based drilling muds, however, increase the total gamma-ray count rate considerably. In the present study, the polymer/bentonite drilling mud was used in corings. Cavings and casings can cause underestimation while interpreting a gamma-ray log. Intervals having a lot of cavings contain more drilling mud between the gamma ray detector and the formation, which attenuates the gamma radiation produced by the formation [12]. The gamma count rate by logging carried out using the metal or cement casing is lower than usually accepted. In the present study, the metal casing was used in all analysed boreholes except one. Wells were cased at a depth of 35.5 to 78.0 m mostly in the unstable part of OB.

Raw data were provided by APCO and served as a basis for the present analysis. The gamma-ray log is reported in American Petroleum Institute (API) units, which are defined empirically by calibration to a reference well at the University of Houston, USA. In the present work, a scale of 0–800 API units was used. The work was done using a Robertson Geologging 3-arm Caliper Sond (UK) equipped with a natural gamma ray detector (50 × 25 mm NaI(Tl) scintillation crystal). The body length of the sond was 2.12 m and its diameter 38 mm. During the measurements, the caliper, however, was not in the measuring position. Thus, the data were not corrected against the diameter of drill holes. Gamma radiation measurements in boreholes were taken every cm. A slow logging speed of 4.5–5.5 m/min (7.5–9.2 cm/s) was used in order to avoid the instability of borehole walls. Such a technique would provide a bed-resolution of 15 to 30 cm [13].

The Jordan Oil Shale Company studied the chemical composition of OS of three drill-core samples (BH-1, BH-3, BH-5). Whole-rock geochemical analyses of major and trace elements were carried out at the Institute of Geology, Tallinn University of Technology, Estonia. A set of 40 elements (usually 12 major and 28 trace elements) of up to 2 m long drill-core samples were analysed by X-ray fluorescence (XRF) and X-ray diffraction (XRD) methods. In this work, data on apatite and uranium contents are compared with information obtained by gamma logs.

3. Methods

First, individual raw gamma logs were compared with each other and litho-stratigraphic boundaries to find out similarities and general long wavelength trends. For that, the thicknesses of individual layers were normalized against the average layer thicknesses that were calculated as median values of the thicknesses of 16 individual layers. A constant spacing of 1 mm (in depth)

between the sampling points in the series was generated by linear interpolation and the average and median values of natural gamma intensity were calculated for every mm.

Second, gamma radiation bar logs were produced. For that, simple moving averages (SMA) with radiuses of 1 and 2.5 m based on raw gamma-ray data were calculated for every mm in depth. The radiuses were chosen using the trial-and-error method. Being applied to any averaging method, the method used is subjective but the chosen radiuses were found to still provide details good enough to enable identification of the signals of about 1 m thick dolomitic interlayers. Then, the values averaged with a radius of 1 m were subtracted from those averaged with a radius of 2.5 m. White and black stripes were applied to negative and positive differences, respectively. Thus, based on a simple positive-negative relationship, a binary bar log was produced for every borehole, and compared against the location of boundaries from lithostratigraphic studies. Such a method describes the relative changes of gamma radiation with no consideration of its absolute values, which vary from borehole to borehole. The individual bar codes were numbered and similarities between the logs from individual boreholes were visually identified to create an average bar log that would act as a basis for identification of stratigraphic boundaries from gamma-ray data alone.

Third, a blind experiment was performed to validate the results by comparing the average bar log data with information on three gamma-ray logs without prior knowledge of stratigraphy.

4. Results

The OS seam can be distinguished from footwall (FW; chert with < 10 cm thick interbeds of phosphatic mudstone and calcitic veins) and overburden (chalk and chalky limestone with minor chert) by significantly higher API values (Fig. 2, Table 1). Within the lithostratigraphic layer A (very fine phosphatic laminite mudstone with wackestone, numerous apatite concretions, and chert) that composes the lowermost 10.24 m thick layer of the deposit (here and below median values of the studied 16 boreholes are given; see Table 1), the gamma-ray logging values decrease from bottom to top (Fig. 2). Characteristic is a high amplitude spike in the bottom of the layer. It corresponds to bar code A1 (Fig. 3a) and is well visible in most of the boreholes that reach FW. In addition to A1, codes a1, A2, a2 and A3 are associated with the layer. The thin (0.71 m) diagenetic dolomitic limestone interlayer A/B has a low NGAM value that is often indicative for the layer. It is always associated with code a3 (Fig. 3). Usually, A/B is associated with the middle or upper part of code a3 as the code is wider (2.36 m; Table 1) than the interlayer itself. Layer B1 (very fine laminite mudstone with wackestone, numerous apatite concretions, and minor chert; 7.37 m in thickness)
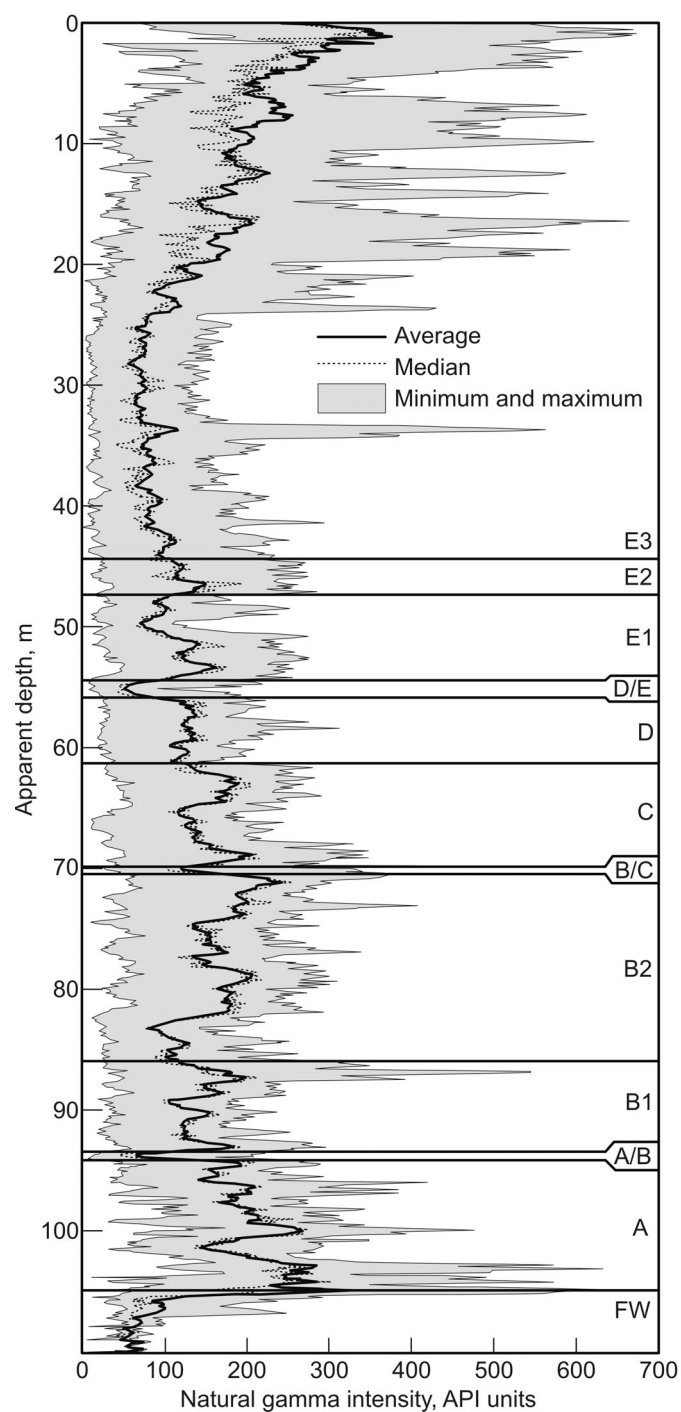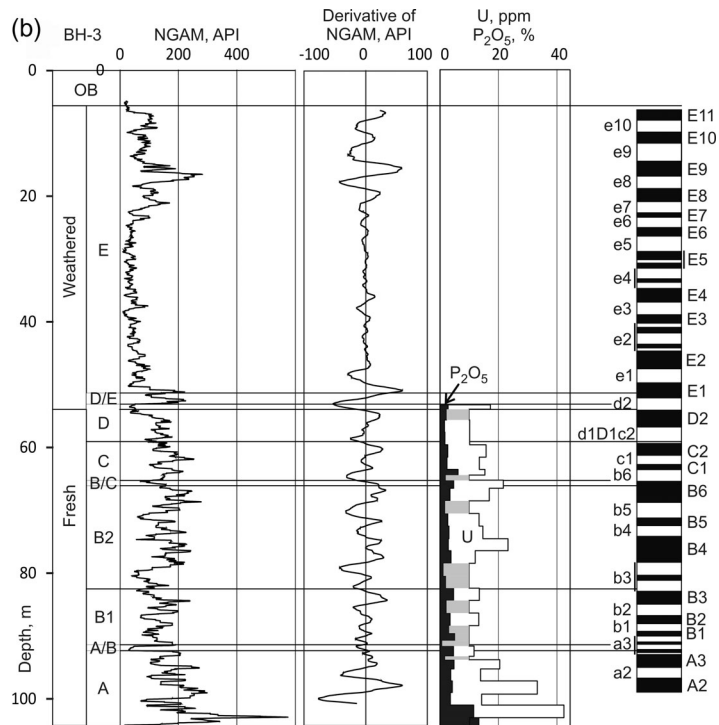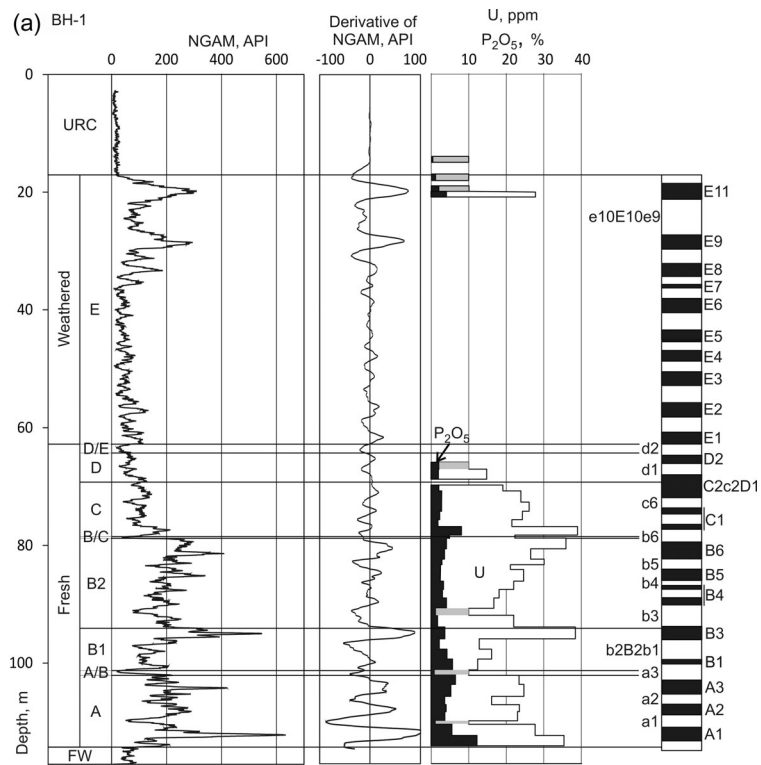
Fig. 2. Average and median of natural gamma-ray logs based on data about 16 individual boreholes. Depth scale is normalized against the average thickness of oil shale layers. (FW – footwall; A–E3 – oil shale and diagenetic dolomitic limestone interlayers.)
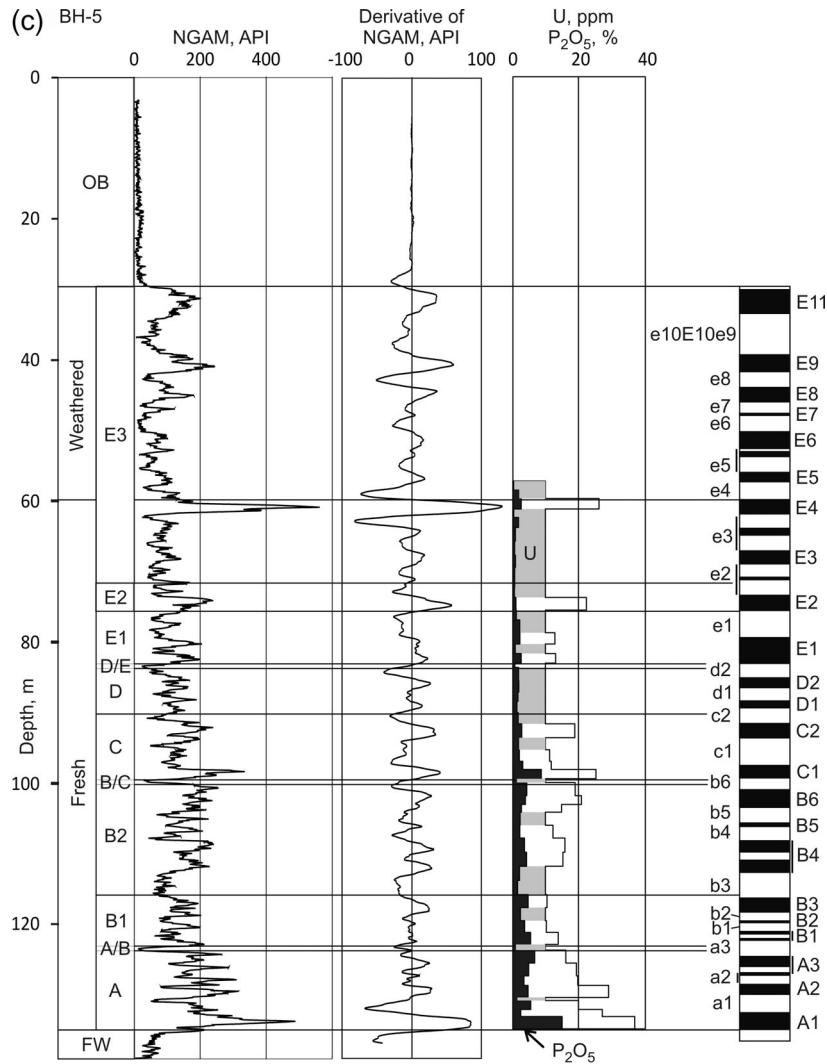
(to be continued)

Fig. 3. Data about boreholes: (a) BH-1, (b) BH-3, (c) BH-5. From left to right of each subfigure: (i) lithostratigraphic data (see Introduction and [10] for layers characteristics), (ii) gamma-ray logging data (NGAM) in API units, (iii) averaged NGAM that represents a derivative of NGAM as obtained by subtracting a simple moving average with a radius of 1 m from that with a radius of 2.5 m, (iv) content of U (grey columns indicate results below analytical limit, 10 ppm) and P_2O_5 (black columns), (v) a set of bar log with codes.

overlies A/B. Within the layer the NGAM values decrease with depth (Fig. 3a) or show no specific trend (Figs. 3a–b). The layer is characterized by five codes: B1, b1, B2, b2, B3. NGAM suffers a sudden decrease at the upper boundary of layer B1, producing almost a perfect concurrence of code B3 with lithological boundary. The lowermost part of the 15.54 m layer B2

(very fine laminite mudstone with wackestone, rare chert, and small calcite concretions in the base) has characteristic low NGAM values corresponding to the 4.30 m thick (Table 1) code b3 (Fig. 3). A minor positive excursion may occur within b3 (Fig. 3b). The boundary between codes b3 and B4, which is 4.13 m thick, is marked by a sharp increase in gamma intensity. The upper part of the layer starts with a small trough (code b4) having low values of NGAM intensity, after which the values increase (codes B5, b5 and B6; Table 1, Fig. 3). The 0.61 m thick diagenetic dolomitic limestone interlayer B/C is associated with a characteristic negative spike and the 1.76 m thick code b6. Usually, the interlayer is located in the middle of the code (Figs. 3a–c) but is not always well seen as is overlapped by the neighboring codes B6 (Fig. 3b) and C1. The very fine laminite mudstone layer C (thickness 9.10 m) with some wackestone is identifiable by a characteristic trough in the gamma-ray signal, whose NGAM intensity is generally lower in the middle of the layer and higher in its edges (Figs. 2 and 3c). Such a relationship, however, is not always obvious (Figs. 3a–b). The layer is associated with the upper part of codes b6, C1, c1 and C2, and the lower part of c2. The maximum amplitude of gamma ray intensity associated with code C1 is usually somewhat larger than that associated with C2, but this may be vice versa as well. Code C2 is thicker (2.18 m) than C1 (1.83 m). Code c1 is also relatively thick (2.94 m; Table 1). The NGAM intensity curve associated with the very fine 5.23 m laminite mudstone layer D with some wackestone is relatively steady (Fig. 2). However, the NGAM intensity curves for a few boreholes exhibit some change, decreasing or increasing with depth (Fig. 3a). The layer is associated with the middle and upper parts of c2, full codes D1, d1 and D2, and, occasionally, the lower part of d2 (for median thicknesses see Table 1). Code d2 is associated with the diagenetic dolomitic limestone interlayer D/E but is thicker than the 1.40 m layer itself.

The fine laminite mudstone oil shale E layer with some wackestone is located at the top of interlayer D/E. Stratigraphically, E is divided into three sublayers from bottom to top: E1, E2, E3 (see Table 1 for the data). There are, however, no data on the exact location of boundaries between the sublayers for half (eight) of the boreholes analyzed. The large wavelength component of the gamma-ray intensity curve shows first an upward decrease in the deepest part of layer E (corresponding to layers E1, E2 and the lowermost part of E3; Figs. 2, 3a–b). The layer's middle part is characterized by low natural gamma intensity values and gradients. The upper part of layer E consists of high amplitude spikes and shows relatively high gamma-ray intensity values. The layer is characterized by 21 codes. The relatively wide codes E1 and e1 (2.59 and 3.12 m in thickness, respectively; Table 1) are associated with the lithostratigraphic layer E1 due to the gamma ray intensity which is high in the lower part of layer E1 and low in its higher part. The lithostratigraphic layer E2 is most often connected with a high amplitude spike corresponding to code E2 (Fig. 3c). The codes of both signs from e2 to e6 (the lithostratigraphic layer E3) are based on the low-value gamma signal

and are of variable thickness. In contrast, there are high gradients in the upper part of layer E3 corresponding to codes (both signs) E7–E11. The OS seam in the location of two boreholes (BH-15 and BH-16) has likely suffered some MCM Formation erosion as several topmost codes are missing.

5. Discussion

The Maastrichtian oil shales in the Middle East have been formed in an extensive upwelling system that operated along the south-eastern margins of the shrinking Tethys Ocean [14]. OS is mainly of marine algal origin and was formed with high organic input in low-oxygen conditions and was efficiently buried [15, 16]. Considering possible sources of radioactivity (U, Th, K), several studies [17–19] have noted a positive correlation between organic matter and uranium contents. The possible phases hosting U are apatite supergroup minerals that form due to bacterial activity under anoxic conditions [20].

The highs and lows of the gamma curve positively correlate with the contents of U and P_2O_5 (Fig. 3). Also, there is a positive moderate correlation between apatite and U contents ($r \approx 0.6$; not taking into consideration results below analytical limit, U < 10 ppm), which suggests that gamma logs reflect the concentration of U in apatite. The lateral uniformity of the apatite content in OS layers causing regular gamma radiation patterns forms a basis for deposit-wide stratigraphic correlations by using gamma logs.

The boundary between WOS and FOS is often located within layer E, but may be situated lower as well. As seen in about half of the boreholes (see Fig. 3c), the irregular high gamma-ray intensity anomaly is associated with the boundary between WOS and FOS. Thus the anomaly may be of secondary origin due to mobilization of U in oxic conditions and its redistribution into FOS. In case of BH-5, no prominent content of P_2O_5, but U, is associated with such a gamma-ray anomaly, supporting the above idea of U mobilization and resettling. According to Yang et al. [21], OM together with humic acids may play a significant role in uranium enrichment. Uranium occurs naturally in both the U^{4+} and U^{6+} valence states. Cation U^{4+}, which is a mobile form of uranium, tends to react with free oxygen to form UO_2^{+2}. In the transitional zone from the oxidizing to reducing conditions, UO_2^{+2} is mostly reduced to U^{4+} and settles.

Because of the possibility for such an unusual positive peak, interpretation of gamma-ray data collected near the boundary between WOS and FOS is complicated, affording too thick or too thin bar codes. To minimize the effect of such extremes, median, not average, values were used in calculations of the summarized code (Table 1, Fig. 4). On the hand, we note that even if such a positive gamma-ray peak exists at the WOS-FOS boundary, the above peaks are identifiable, suggesting that some of the causes of

gamma radiation may have survived in the process of weathering. It enables internal stratification of layer E and definition of the boundary between WOS and OB.

Comparison of individual codes with median ones, each other and litho-stratigraphic data is illustratively shown in Figure 4. As seen from the figure, the codes, once defined on the basis of their succession, thickness and amplitude (Table 1), allow localization of lithostratigraphic boundaries with some certainty. One has to pay attention to the following regularities: (i) the OS seam is bordered by high amplitude codes A1 (lower) and E11 (upper), (ii) layer A extends to the middle of code a3, (iii) interlayer A/B is associated with code a3 but is thinner, (iv) layer B1 extends from the upper part of code a3 up to B3. The boundary between layers B1 and B2 is likely to be defined by the boundary between codes B3 and b3, (v) layer B2
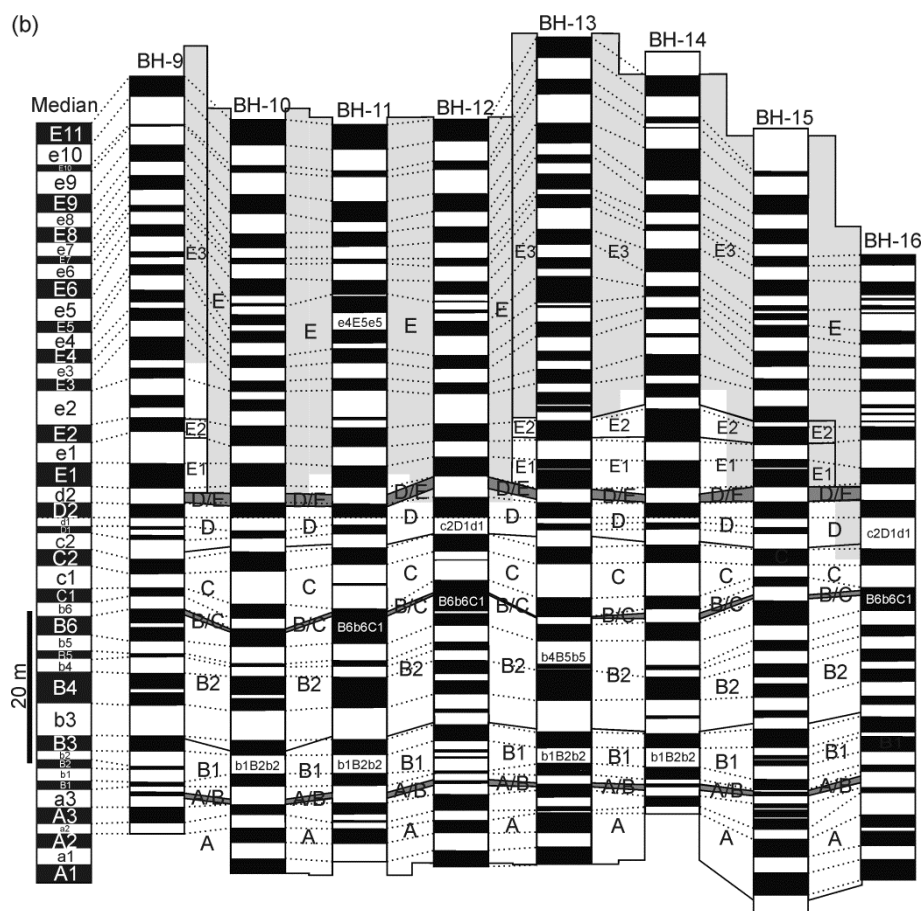

(to be continued)

(b)
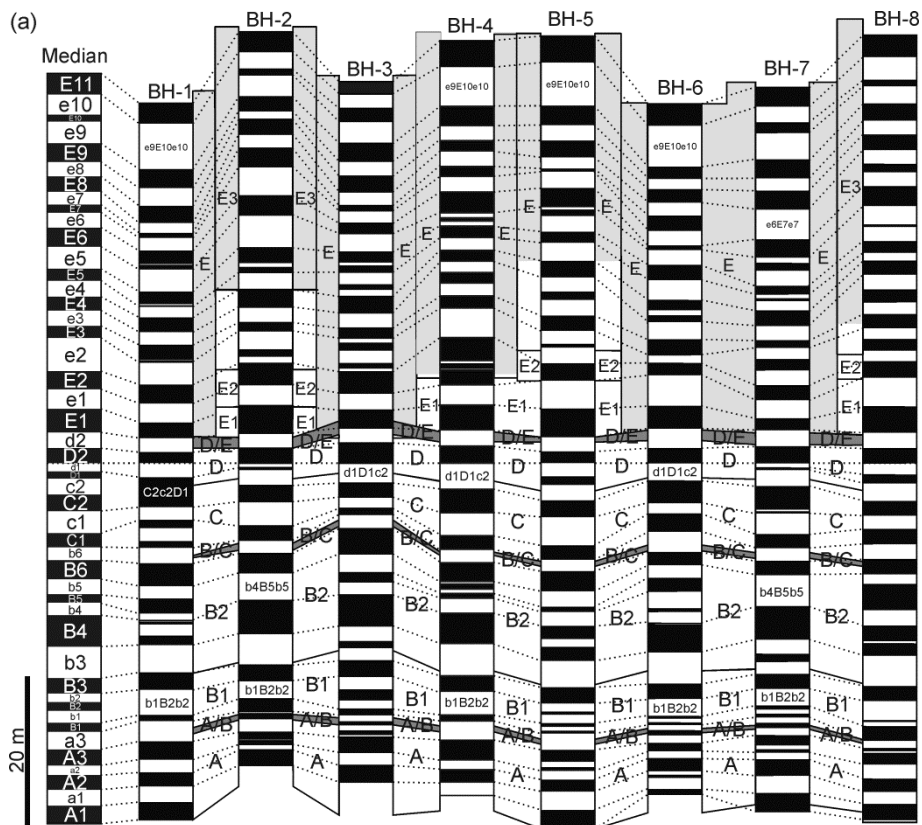
Fig. 4. (a), (b): Gamma-ray intensity based bar logs compared with the median log (on the left). Lithostratigraphic layers (see Introduction and [10]; light and dark grey colours indicate weathered OS and dolomitic interlayers, respectively) are given in between the logs. Individual interpretation of BH-1, BH-3 and BN-5 is illustrated in Figure 3.

extends from b3 to b6, (vi) interlayer B/C is associated with b6, but is thinner than the code, (vii) layer C extends from b6 to C2, (iix) layer D extends from c2 to D2, (ix) interlayer D/E is associated with code d2 and is likely of the same thickness, (x) layer E1 is associated with codes E1 and e1, (xi) layer E2 is likely at the same depth as code E2, (xii) layer E3 is associated with codes e2–E11, in case the seam has suffered erosion, the topmost high amplitude codes E7–E11 are (partly) missing, and (xiii) unusual high peaks could correspond to the boundary between WOS and FOS.

The above scheme was tested by calculating gamma log based bar codes and interpreting them for three boreholes without prior knowledge of their lithological sequence. The test results (Fig. 5) can be considered reliable as
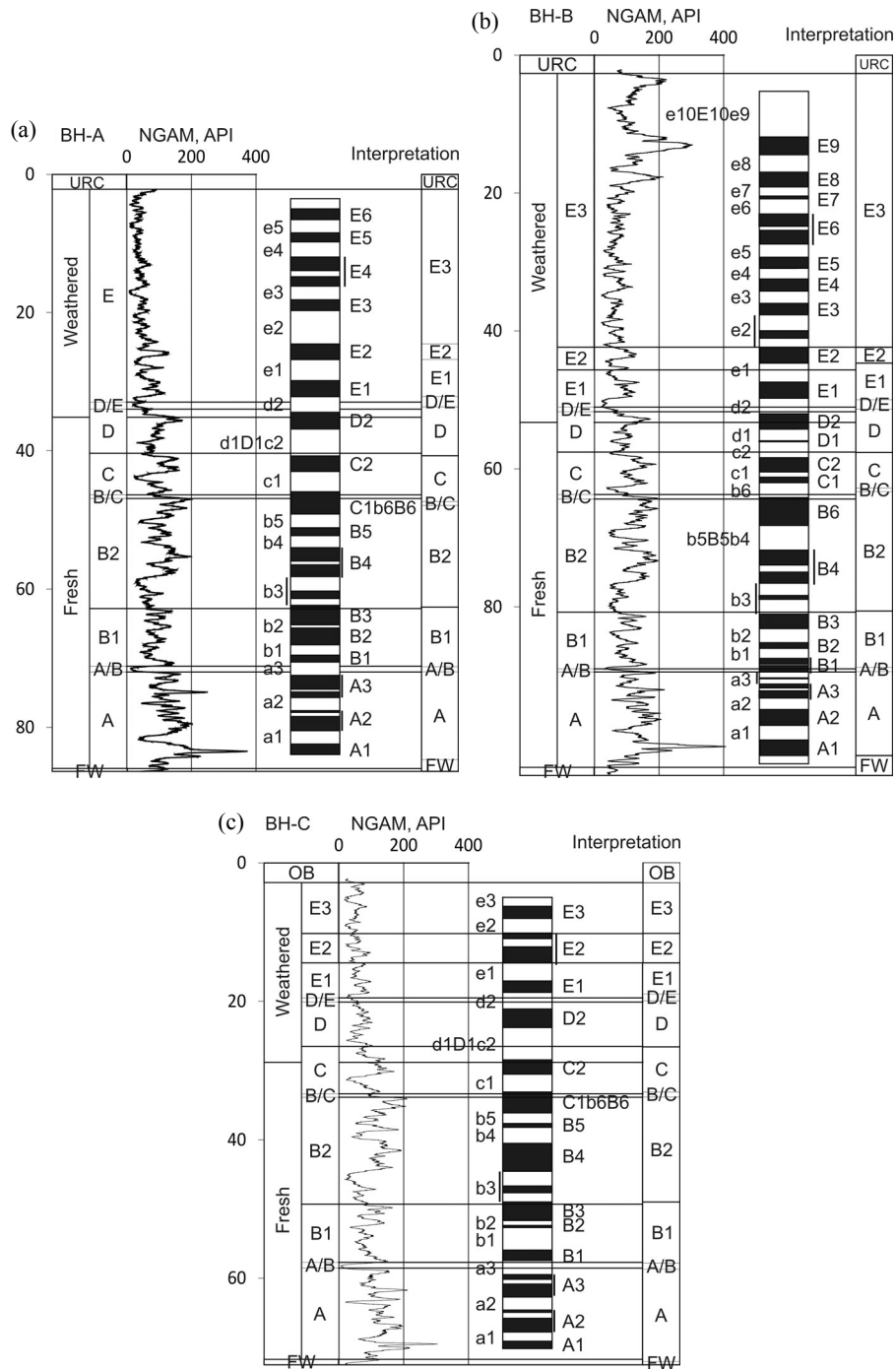
Fig. 5. Test data about boreholes: (a) BH-A, (b) BH-B, (c) BH-C. From left to right of each subfigure: (i) lithostratigraphic data (see Introduction and [10] for layers characteristics), (ii) gamma-ray logging data (NGAM) in API units, (iii) bar log, (iv) test data: lithostratigraphic scheme based on (ii) and (iii) without prior knowledge of (i).

the scheme enables determination of stratigraphic boundaries between the layers with sufficient accuracy (with a precision generally < 1 m; the standard error of predicted depths ≤ 0.76 m; Table 2). This is comparable to the precision of depth estimation during the process of drilling. The scheme provided in the present work can be used as a basis for interpreting new logs in the Attarat Um Ghudran deposit in future. Thus, in later exploration stages some of the expensive core drillings can be replaced with cheaper percussion drilling combined with gamma-ray logging.

Table 2. Interpreted (Test) and real (Real) depths of lower boundaries of specific layers, and depth differences (Diff.) between the tested boreholes

Bore-hole	Depth, m								
	BH-A			BH-B			BH-C		
Layer	Test	Real	Diff.	Test	Real	Diff.	Test	Real	Diff.
AE				2.60	n.d.		2.77	n.d.	
E3	24.49	n.d.		42.24	42.27	−0.03	10.11	n.d.	
E2	26.74	n.d.		44.55	45.65	−1.10	14.37	n.d.	
E1	32.10	32.92	−0.82	49.86	51.04	−1.18	18.84	19.5	−0.66
D/E	33.59	33.94	−0.35	51.22	51.65	−0.43	19.83	20.1	−0.27
D	40.56	40.30	0.26	57.49	57.55	−0.06	26.49	26.5	−0.01
C	47.24	46.29	0.95	62.66	63.70	−1.04	33.01	33.35	−0.34
B/C	47.78	46.80	0.98	63.17	64.30	−1.13	33.74	33.85	−0.11
B2	62.48	62.72	−0.24	80.46	80.74	−0.28	48.85	49.25	−0.40
B1	71.08	71.05	0.03	88.63	88.95	−0.32	57.68	57.66	0.02
A/B	71.82	71.94	−0.12	89.23	89.36	−0.13	58.58	58.49	0.09
A	84.50	85.85	−1.35	101.40	103.22	−1.82	71.88	71.66	0.22
Average			−0.07			−0.71			−0.16
Minimum difference			−1.35			−1.82			−0.66
Maximum difference			0.98			−0.03			0.22
Standard error of the predicted depth			0.76			0.61			0.21

n.d. = not determined

6. Conclusions

Gamma-ray logging increases the reliability of identification of stratigraphic units in borehole sequences, especially in the case of rotary or percussion drilling with no drill-core available for lithostratigraphic determinations. In the Attarat Um Ghudran deposit, the oil shale seam (both the weathered and fresh oil shale) is more radioactive than the underlying chert and overlying chalk and chalky limestone layers. The highs and lows of the oil shale gamma curve positively correlate with the contents of U and P_2O_5. Also, there is a positive correlation between apatite and U values, suggesting that the gamma logs reflect mostly the concentration of U in apatite. The lateral uniformity of the apatite content forms a basis for deposit-wide stratigraphic correlations with the help of gamma logs.

The high gamma-ray intensity anomaly may be associated with the boundary between the weathered and fresh oil shale, pointing to the mobilization of some U in oxic conditions and resettling in fresh oil shale. Mobilization has, however, not been comprehensive as gamma-ray peaks within the weathered oil shale are still recognizable.

The presented gamma log based bar code scheme may provide a possibility for deposit-wide correlations. The scheme enables determination of stratigraphic boundaries of layers with reasonable accuracy (the standard error of predicted depths $\leq$ 0.76 m). In detailed exploration stages, percussion drilling combined with gamma-ray logging is sufficiently credible.

Acknowledgements

REFERENCES

1. *Independent Statistics and Analysis.* U.S. Energy Information Administration, 2014. URL: http://www.eia.gov/beta/international/country.cfm?iso=JOR (accessed Aug 12, 2015).
2. Hrayshat, E. S. Oil shale – an alternative energy source for Jordan. *Energ. Source. Part A,* 2008, **30**(20), 1915–1920.
3. Knaus, E., Killen, J., Biglarbigi, K., Crawford, P. An overview of oil shale resources. In: *Oil Shale: A Solution to the Liquid Fuel Dilemma*, ACS Symposium Series, 2010, **1032**, 3–20.
4. Al-Zoubi, A., Ben Avraham, Z. Structure of the earth's crust in Jordan from potential field data. *Tectonophysics,* 2002, **346**, 45–59.
5. Alqudah, M., Hussein, M. A., van der Boorn, S., Podlaha, O. G., Mutterlose, J. Biostratigraphy and depositional setting of Maastrichtian - Eocene oil shales from Jordan. *Mar. Petrol. Geol.,* 2015, **60**, 87–104.
6. Alali, J., Salah, A. A., Yasin, S. M., Omari, W. A. *Geological Survey Administration. Mineral Status and Future Opportunity. Oil Shale.* Report, 2006. URL: http://www.nra.gov.jo/images/stories/pdf_files/Oil_Shale.pdf (accessed Apr 22, 2014).
7. Sunna, B. F. *Attarat Um Ghudran Oil Shale Deposit.* Natural Resources Authority, Ministry of Energy and Mineral Resources, The Hashemite Kingdom of Jordan, 1984 (unpublished report).
8. Hamarneh, Y. *Oil Shale Resources Development in Jordan.* Report, 1988. URL: http://www.nra.gov.jo/images/stories/pdf_files/Updated_Report_2006.pdf (accessed Apr 22, 2014).
9. Voolma, M., Soesoo, A., Puura, V., Hade, S., Aosaar, H. Assessing the geochemical variability of oil shale in the Attarat Um Ghudran deposit, Jordan. *Est. J. Earth Sci.*, 2016, **65**(2), 61–74.
10. Puura, V., Soesoo, A., Voolma, M., Hade, S., Aosaar, H. Chemical composition

of the mineral matter of the Attarat Um Ghudran oil shale, Central Jordan. *Oil Shale*, 2016, **33**(1), 18–30.

11. Hutton, A. C. Petrographic classification of oil shales. *Int. J. Coal Geol.,* 1987, **8**(3), 203–231.

12. Sharma, P. V. *Environmental and Engineering Geophysics*. Cambridge University Press, Cambridge, 1997.

13. Lehmann, K. Environmental corrections to gamma-ray log data: Strategies for geophysical logging with geological and technical drilling. *J. Appl. Geophys.,* 2010, **70**(1), 17–26.

14. Almogi-Labin, A., Flexer, A., Honigstein, A., Rosenfeld, A., Rosenthal, E. Biostratigraphy and tectonically controlled sedimentation of the Maastrichtian in Israel and adjacent countries. *Revista Española de Paleontologia,* 1990, **5**(1), 41–52).

15. Meilijson, A., Ashckenazi-Polivoda, S., Ron-Yankovich, L., Illner, P., Alsenz, H., Speijer, R. P., Almogi-Labin, A., Feinstein, S., Berner, Z., Püttmann, W., Abramovich, S. Chronostratigraphy of the Upper Cretaceous high productivity sequence of the southern Tethys, Israel. *Cretaceous Res.*, 2014, **50**, 187–213.

16. Schneider-Mor, A., Alsenz, H., Ashckenazi-Polivoda, S., Illner, P., Abramovich, S., Feinstein, S., Almogi-Labin, A., Berner, Z., Püttmann, W. Paleoceanographic reconstruction of the late Cretaceous oil shale of the Negev, Israel: Integration of geochemical, and stable isotope records of the organic matter. *Palaeogeogr., Palaeocl.*, 2012, **319-320**, 46–57.

17. Moh'd, B. K., Powell, J. H. Uranium distribution in the Upper Cretaceous-Tertiary Belqa Group, Yarmouk Valley, Northwest Jordan. *Jordan Journal of Earth and Environmental Sciences,* 2010, **3**(1), 49–62.

18. Swanson, V. E. *Oil Yield and Uranium Content of Black Shales*. Geological Survey Professional Paper 356-A, United States Government Printing Office, Washington, 1960.

19. Tzifas, I. Tr., Godelitsas, A., Magganas, A., Androulakaki, E., Eleftheriou, G., Mertzimekis, T. J., Perraki, M. Uranium-bearing phosphatized limestones of NW Greece. *J. Geochem. Explor.,* 2014, **143**, 62–73.

20. Goldhammer, T., Brüchert, V., Ferdelman, T. G., Zabel, M. Microbial sequestration of phosphorus in anoxic upwelling sediments. *Nat. Geosci.,* 2010, **3**, 557–561.

21. Yang, H., Zhang, W., Wu, K., Li, S., Peng, P., Qin, Y. Uranium enrichment in lacustrine oil source rocks of the Chang 7 member of the Yanchang Formation, Erdos Basin, China. *J. Asian Earth Sci.*, 2010, **39**(4), 285–293.